An Algebraic Solver for the Oseen Problem with Application to Hemodynamics

Igor N. Konshin, Maxim A. Olshanskii and Yuri V. Vassilevski

Abstract The paper studies an iterative method for algebraic problems arising in numerical simulation of blood flows. Here we focus on a numerical solver for the fluid part of otherwise coupled fluid-structure system of equations which models the hemodynamics in vessels. Application of the finite element method and semi-implicit time discretization leads to the discrete Oseen problem at every time step of the simulation. The problem challenges numerical methods by anisotropic geometry, open boundary conditions, small time steps and transient flow regimes. We review known theoretical results and study the performance of recently proposed preconditioners based on two-parameter threshold ILU factorization of non-symmetric saddle point problems. The preconditioner is applied to the linearized Navier–Stokes equations discretized by the stabilized Petrov–Galerkin finite element (FE) method. Careful consideration is given to the dependence of the solver on the stabilization parameters of the FE method. We model the blood flow in the digitally reconstructed right coronary artery under realistic physiological regimes. The paper discusses what is special in such flows for the iterative algebraic solvers, and shows how the two-parameter ILU preconditioner is able to meet these specifics.

Keywords Hemodynamics · Iterative methods · Threshold ILU factorization · Navier–Stokes equations · Finite element method · SUPG stabilization

I. N. Konshin · Y. V. Vassilevski (✉)
Institute of Numerical Mathematics of the Russian Academy of Sciences, Moscow, Russia
e-mail: yuri.vassilevski@gmail.com

M. A. Olshanskii
Department of Mathematics, University of Houston, Houston, USA
e-mail: molshan@math.uh.edu

I. N. Konshin
Dorodnicyn Computing Centre, FRC CSC RAS, Moscow, Russia
e-mail: igor.konshin@gmail.com

Y. V. Vassilevski
Moscow Institute of Physics and Technology, Moscow, Russia

Y. V. Vassilevski
I.M. Sechenov First Moscow State Medical University, Moscow, Russia

B. N. Chetverushkin et al. (eds.), *Contributions to Partial Differential Equations and Applications*, Computational Methods in Applied Sciences 47,
https://doi.org/10.1007/978-3-319-78325-3_18

1 Introduction

Numerical simulations play an increasing role in visualization, understanding and predictive modelling of many biological flows, including blood flow in arteries and the heart. The efficiency of a numerical approach depends on the right choice of mathematical model, its discretization and the algebraic solvers used to compute the solution to a discrete model. For the blood flow simulations, state-of-the-art methods are built on a fluid-structure interaction (FSI) model which typically includes equations describing the motion of Newtonian viscous fluid, equations for an elastic structure and coupling conditions [5]. In the process of numerical integration of the FSI system, however, one often decouples the fluid equations from the elasticity equations on every time step and hence applies segregated algebraic solvers for each of the decoupled problem, see, e.g., [12]. Furthermore, for the reason of time-sensitivity of simulations or the ambiguity of the information regarding the properties of the structure, hemodynamic simulations are often performed in a fixed geometries, i.e. the vessels wall is assumed to be rigid rather than elastic. In both cases, one is interested in an efficient numerical solve for the Navier–Stokes equations describing the motion of incompressible Newtonian fluids in a bounded domain $\Omega \subset \mathbb{R}^3$ and time interval $[0, T]$:

$$\begin{cases} \dfrac{\partial \mathbf{u}}{\partial t} - \nu \Delta \mathbf{u} + (\mathbf{u} \cdot \nabla)\mathbf{u} + \nabla p = \mathbf{f} & \text{in } \Omega \times (0, T], \\ \operatorname{div} \mathbf{u} = 0 & \text{in } \Omega \times [0, T], \\ \mathbf{u} = \mathbf{g} & \text{on } \Gamma_0 \times [0, T], \\ -\nu(\nabla \mathbf{u}) \cdot \boldsymbol{n} + p\boldsymbol{n} = \mathbf{h} & \text{on } \Gamma_{\mathrm{N}} \times [0, T], \\ \mathbf{u}(\mathbf{x}, 0) = \mathbf{u}_0(\mathbf{x}) & \text{in } \Omega. \end{cases} \tag{1}$$

The unknowns are the velocity vector field $\mathbf{u} = \mathbf{u}(\mathbf{x}, t)$ and the pressure field $p = p(\mathbf{x}, t)$. The volume forces $\mathbf{f}$, boundary and initial values $\mathbf{g}$, $\mathbf{h}$ and $\mathbf{u}_0$ are given. Parameter ν is the kinematic viscosity; the boundary of the domain is decomposed as $\partial\Omega = \overline{\Gamma}_0 \cup \overline{\Gamma}_{\mathrm{N}}$ with Dirichlet part $\Gamma_0 \neq \varnothing$ and Neumann part Γ_{N}. An important parameter of the flow is the dimensionless Reynolds number $\mathrm{Re} = UL/\nu$, where U and L are characteristic velocity and linear dimension.

The Navier–Stokes equations (1) are fundamental equations of fluid mechanics and are central for modelling of many physical phenomena. In hemodynamic applications, one may point to several special features of otherwise general fluid flow problem in (1):

(i) Anisotropic geometry. The domain Ω typically represents a blood vessel, which is a stretched branching object;
(ii) Open boundaries of mixed type. The computational domain has artificial (open) boundaries, where the vessel is cut. Depending on the stage of cardiac cycle, forward and reverse flows may happen through the same part of the open boundary, leading to the boundary changing type outflow/inflow;

(iii) Different flow regimes. Variable blood flux generated over one heartbeat may produce flows with varying Reynolds numbers from laminar to transitional;
(iv) Finite element method prevails. Due to complex geometry and coupling to elasticity equations, finite element method is the very common choice for discretization of (1) in hemodynamic applications. A regularization (in the form of least-square terms or a sub-grid model) is often added to stabilize the FE method for higher Reynolds numbers;
(v) Small time steps. The physics of the problem dictates small time steps of order $10^{-3} \times$ cardiac cycle time for the numerical integration of (1).

Semi-implicit time discretization or an implicit one combined with the linearization of the Navier–Stokes system (1) by Picard fixed-point iteration result in a sequence of Oseen problems of the form

$$\begin{cases} \alpha\mathbf{u} - \nu\Delta\mathbf{u} + (\mathbf{w}\cdot\nabla)\mathbf{u} + \nabla p = \hat{\mathbf{f}} & \text{in } \Omega, \\ \operatorname{div}\mathbf{u} = \hat{g} & \text{in } \Omega, \\ \mathbf{u} = \mathbf{0} & \text{on } \Gamma_0, \\ -\nu(\nabla\mathbf{u})\cdot\boldsymbol{n} + p\boldsymbol{n} = \mathbf{0} & \text{on } \Gamma_{\mathrm{N}}, \end{cases} \tag{2}$$

where $\mathbf{w}$ is a known velocity field from a previous iteration or time step and α is proportional to the reciprocal of the time step. Non-homogeneous boundary conditions in the nonlinear problem are accounted in the right-hand side of (2). A finite element spatial discretization of (2) produces large sparse systems of the form

$$\begin{pmatrix} A & \widetilde{B}^T \\ B & -C \end{pmatrix} \begin{pmatrix} u \\ p \end{pmatrix} = \begin{pmatrix} f \\ g \end{pmatrix}, \tag{3}$$

where u and p represent the discrete velocity and pressure, respectively; $A \in \mathbb{R}^{n\times n}$ is the discretization of the diffusion, convection, and time-dependent terms. The matrix A accounts also for certain stabilization terms. Matrices B and $\widetilde{B}^T \in \mathbb{R}^{n\times m}$ are (negative) discrete divergence and gradient. These matrices may also be perturbed due to stabilization. It is typical for the stabilized methods that $B \neq \widetilde{B}$, while for a plain Galerkin method these two matrices are the same. Matrix $C \in \mathbb{R}^{m\times m}$ results from possible pressure stabilization terms, and f and g contain forcing and boundary terms. For the LBB stable finite elements, no pressure stabilization is required and so $C = 0$ holds. If the LBB condition is not satisfied, the stabilization matrix $C \neq 0$ is typically symmetric and positive semidefinite. For $B = \widetilde{B}$ of the full rank and positive definite $A = A^T$ the solution to (3) is a saddle point.

Considerable work has been done in developing efficient preconditioners for Krylov subspace methods applied to system (3) with $\widetilde{B} = B$; see the comprehensive studies in [4, 8, 19] of the preconditioning exploiting the block structure of the system. Several algebraic solvers were specifically designed or numerically tested

for solving (3) resulting from hemodynamic applications. This includes incomplete block LU factorizations mimicking pressure correction splitting methods on the algebraic level [20], block-triangular preconditioners based on approximation of pressure advection–diffusion operator [18], additive Schwartz preconditioner [7], relaxed dimensional factorization block preconditioner [3], see also [7] for the numerical comparison of several preconditioners for the hemodynamic simulations.

The special features of blood flow problems discussed above impact the algebraic properties of the discrete system (3), and ideally, an efficient solver accounts for them. Thus, the inf-sup stability constants of velocity–pressure elements strongly depend on the anisotropy of domain Ω, see [6]. This may lead to poor performance of preconditioners based on pressure Schur complement approximations. Reversed flows through the open boundary is an energy increasing and de-stabilizing phenomenon, potentially resulting in the lost of ellipticity by the A block of (3). Next, different flow regimes require a robust preconditioner with respect to the variation of the Reynolds numbers. Finite element method leads, in general, to matrices with higher fill-in comparing to finite volumes or finite differences schemes. We note that hierarchical tetrahedral grids are rarely used to reconstruct blood vessels. This reduce the applicability of geometric multigrid methods. Furthermore, we shall see that additional terms added to stabilize finite element method for convection dominated flows often make algebraic problem harder to solve. Finally, small time steps suggest that reusable preconditioners and those benefiting from the diagonal dominance in the A-block should be preferred.

In the paper we study the properties of an algebraic solver for (3) based on a Krylov subspace iterative method and a two-parameter ILU preconditioner. The preconditioner results from a special incomplete elementwise LU factorization suggested and studied in [14] for symmetric positive definite matrices and further extended to non-symmetric saddle-point systems in [16, 17]. Here we review the available analysis and discuss how this algebraic solver addresses the challenges posed by hemodynamics applications. Further we simulate the blood flow in the digitally reconstructed part of the right coronary artery. Here we experiment with various grids, Reynolds numbers and finite element method stabilization parameters to assess the numerical properties for the iterative method.

The remainder of the paper is organized as follows. In Sect. 2 we give necessary details of the finite element method. Section 3 reviews known stability of the exact LU factorizations for (3). These results are formulated in terms of the properties of the (1,1)-block A, auxiliary Schur complement matrix $BA^{-1}B^T + C$, and the perturbation matrix $B - \widetilde{B}$. In Sect. 4, we formulate the properties of these matrices in terms of problem coefficients and parameters of the FE method. In Sect. 5, we briefly discuss the implication of these results on the stability of a two-parameter variant of the threshold ILU factorization for non-symmetric non-definite problems. In Sect. 6 we study the numerical performance of the method on the sequence of linear systems appearing in simulation of a blood flow in a right coronary artery. Conclusions are collected in the final Sect. 7.

2 Finite Element Method

We assume T_h to be a collection of tetrahedra forming a consistent subdivision of Ω. We also assume for T_h the shape-regularity condition,

$$\max_{\tau \in T_h} \operatorname{diam}(\tau)/\rho(\tau) \leq C_T, \tag{4}$$

where $\rho(\tau)$ is the diameter of the inscribed ball in the tetrahedron τ. A constant C_T measures the maximum anisotropy ratio for T_h. Further we denote $h_\tau = \operatorname{diam}(\tau)$, $h_{\min} = \min_{\tau \in T_h} h_\tau$. Given conforming FE spaces $\mathbb{V}_h \subset (H^1_{\Gamma_0}(\Omega))^3$ and $\mathbb{Q}_h \subset L^2(\Omega)$, the Galerkin FE discretization of (2) is based on the weak formulation: Find $\{\boldsymbol{u}_h, p_h\} \in \mathbb{V}_h \times \mathbb{Q}_h$ such that

$$\begin{aligned} \mathscr{L}(\boldsymbol{u}_h, p_h; \boldsymbol{v}_h, q_h) &= (\hat{\mathbf{f}}, \boldsymbol{v}_h) + (\hat{g}, q_h) \qquad \forall\, \boldsymbol{v}_h \in \mathbb{V}_h,\ q_h \in \mathbb{Q}_h, \\ \mathscr{L}(\boldsymbol{u}, p; \boldsymbol{v}, q) &:= \alpha(\boldsymbol{u}, \boldsymbol{v}) + \nu(\nabla \boldsymbol{u}, \nabla \boldsymbol{v}) + ((\boldsymbol{w} \cdot \nabla)\, \boldsymbol{u}, \boldsymbol{v}) - (p,\ \operatorname{div} \boldsymbol{v}) + (q,\ \operatorname{div} \boldsymbol{u}), \end{aligned} \tag{5}$$

where $(\cdot, \cdot)$ denotes the $L^2(\Omega)$ inner product.

In experiments we use P2-P1 Taylor–Hood FE pair, which satisfies the LBB compatibility condition for $\mathbb{V}_h$ and $\mathbb{Q}_h$ [9] and hence ensures well-posedness and full approximation order for the FE linear problem.

The finite element method (5) needs stabilization or additional subgrid scale modelling if convection terms dominate over the diffusion. We consider one commonly used SUPG stabilization, while more details on the family of SUPG methods can be found in, e.g., [21]. Using (5) as the starting point, a weighted residual for the FE solution multiplied by an 'advection'-depending test function is added:

$$\begin{aligned} \mathscr{L}(\boldsymbol{u}_h, p_h; \boldsymbol{v}_h, q_h) + \sum_{\tau \in T_h} \sigma_\tau (\alpha \boldsymbol{u}_h - \nu \Delta \boldsymbol{u}_h + \boldsymbol{w} \cdot \nabla \boldsymbol{u}_h + \nabla p_h - \boldsymbol{f}, \boldsymbol{w} \cdot \nabla \boldsymbol{v}_h)_\tau \\ = (\boldsymbol{f}, \boldsymbol{v}_h) + (\hat{g}, q_h) \quad \forall \boldsymbol{v}_h \in \mathbb{V}_h,\ q_h \in \mathbb{Q}_h, \end{aligned} \tag{6}$$

with $(f, g)_\tau := \int_\tau fg\, dx$. The second term in (6) is evaluated element-wise for each element $\tau \in T_h$. Parameters σ_τ are element- and problem-dependent. To define the parameters, we introduce mesh Reynolds numbers $\mathrm{Re}_\tau := \|\boldsymbol{w}\|_{L_\infty(\tau)} h_{\boldsymbol{w}}/\nu$ for all $\tau \in T_h$, where $h_{\boldsymbol{w}}$ is the diameter of τ in direction $\boldsymbol{w}$. Several recipes for the particular choice of the stabilization parameters can be found in the literature, see, e.g., [21].

We set

$$\sigma_\tau = \begin{cases} \bar{\sigma} \frac{h_{\boldsymbol{w}}}{2\|\boldsymbol{w}\|_{L_\infty(\tau)}} \left(1 - \frac{1}{\mathrm{Re}_\tau}\right), & \text{if } \mathrm{Re}_\tau > 1, \\ 0, & \text{if } \mathrm{Re}_\tau \leq 1, \end{cases} \qquad \text{with } 0 \leq \bar{\sigma} < 1. \tag{7}$$

Obviously, $\bar{\sigma} = 0$ means that no stabilization is added. The choice of σ_τ in (7) implies the following estimate which we need later in Sect. 6:

$$\sigma_\tau = \bar{\sigma}\frac{h_w}{2\|\boldsymbol{w}\|_{L_\infty(\tau)}}\left(1-\frac{1}{\mathrm{Re}_\tau}\right) \le \bar{\sigma}\frac{h_w}{2\|\boldsymbol{w}\|_{L_\infty(\tau)}}\mathrm{Re}_\tau = \bar{\sigma}\frac{h_w^2}{2\nu} \le \bar{\sigma}\frac{h_\tau^2}{2\nu}. \tag{8}$$

If one enumerates velocity unknowns first and pressure unknowns next, then the resulting discrete system has the 2×2-block form (3) with $C = 0$. The stabilization alters the (1,2)-block of the matrix making the latter not equal to the transpose of the (2,1)-block B. From the available analysis and results of numerical experiments we shall see that the perturbation of A caused by (6) affects the algebraic properties of (3).

3 Some Properties of LU Factorization for (3)

One can think about ILU factorization as a perturbation of exact LU factorization. Hence, it is instructive to have a first look at stability properties of the latter for non-symmetric saddle-point matrices as in (3). The results in this section summarize the analysis in [16, 17], where the reader can find full proofs and further details. The 2×2-block matrix from (3) is in general indefinite and if $C = 0$, its diagonal has zero entries. An LU factorization of such matrices often requires pivoting for stability reasons. However, exploiting the block structure and the properties of blocks A and C, one readily verifies that the LU factorization

$$\mathscr{A} = \begin{pmatrix} A & \widetilde{B}^T \\ B & -C \end{pmatrix} = \begin{pmatrix} L_{11} & 0 \\ L_{21} & L_{22} \end{pmatrix}\begin{pmatrix} U_{11} & U_{12} \\ 0 & -U_{22} \end{pmatrix} \tag{9}$$

with lower (upper) triangle matrices L_{11}, L_{22} (U_{11}, U_{22}) exists without pivoting, once $\det(A) \neq 0$ and there exist LU factorizations for the (1,1)-block

$$A = L_{11}U_{11}$$

and the Schur complement matrix $\widetilde{S} := BA^{-1}\widetilde{B}^T + C$ is factorized as

$$\widetilde{S} = L_{22}U_{22}.$$

Decomposition (9) then holds with $U_{12} = L_{11}^{-1}\widetilde{B}^T$ and $L_{21} = BU_{11}^{-1}$.

Assume A is positive definite. Then the LU factorization of A exists without pivoting. Its numerical stability (the relative size of entries in factors L_{11} and U_{11}) may depend on how large is the skew-symmetric part of A comparing to the symmetric part. More precisely, the following bound on the size of elements of L_{11} and U_{11} holds (see, e.g., (3.2) in [16]):

$$\frac{\||L_{11}||U_{11}|\|_F}{\|A\|} \le n\left(1 + C_A^2\right), \tag{10}$$

where $C_A := \|A_S^{-\frac{1}{2}} A_N A_S^{-\frac{1}{2}}\|$, $A_S = \frac{1}{2}(A + A^T)$, $A_N = A - A_S$. Here and further, $\|\cdot\|$ and $\|\cdot\|_F$ denote the matrix spectral norm and the Frobenius norm, respectively, and $|M|$ denotes the matrix of absolute values of M-entries.

If C is positive semi-definite, $\widetilde{B} = B$, and matrix B^T has the full column rank, then the positive definiteness of A implies that the Schur complement matrix $S := BA^{-1}B^T + C$ is also positive definite. However, this is not the case for a general block $\widetilde{B} \neq B$. The stabilization terms in the finite element method (6) produce the (1,2)-block $\widetilde{B}^T$ which is a *perturbation* of B^T. The positive definiteness of $\widetilde{S} := BA^{-1}\widetilde{B}^T + C$ and the stability of its LU factorization is guaranteed if the perturbation $E = \widetilde{B} - B$ is not too large [17]. In particular, $\widetilde{S}$ is positive definite if the perturbation matrix E is sufficiently small such that it holds

$$\kappa := (1 + C_A)\varepsilon_E c_S^{-\frac{1}{2}} < 1, \tag{11}$$

where $\varepsilon_E := \|A_S^{-\frac{1}{2}} E^T\|$, $c_S := \frac{1}{2}\lambda_{\min}(S + S^T)$. Moreover, if $\widetilde{S}$ is positive definite, the factorization $\widetilde{S} = L_{22}U_{22}$ satisfies the stability bound similar to (10).

The following result about stability of LU factorization of (3) holds.

Theorem 1 *Assume matrix A is positive definite, C is positive semidefinite, and the inequality (11) holds with $\varepsilon_E = \|A_S^{-\frac{1}{2}}(\widetilde{B} - B)^T\|$, $C_A = \|A_S^{-\frac{1}{2}} A_N A_S^{-\frac{1}{2}}\|$, and $c_S = \frac{1}{2}\lambda_{\min}(S + S^T)$, then the LU factorization (9) exists without pivoting. The entries of the block factors satisfy (10) and the following bounds*

$$\frac{\||L_{22}||U_{22}|\|_F}{\|\widetilde{S}\|} \leq m\left(1 + \frac{(1 + \varepsilon_E c_S^{-\frac{1}{2}})C_A}{1 - \kappa}\right),$$

$$\frac{\|U_{12}\|_F + \|L_{21}\|_F}{\|U_{11}\|\|\widetilde{B}\|_F + \|L_{11}\|\|B\|_F} \leq \frac{m(1 + C_A)}{c_A}$$

with $c_A := \lambda_{\min}(A_S)$ and κ from (11).

The above analysis indicates that the LU factorization for (3) exists if the (1,1) block A is positive definite and the perturbation of the (1,2)-block is sufficiently small. The stability bounds depend on the constant C_A which measures the ratio of skew-symmetry for A, the ellipticity constant c_A, the perturbation measure ε_E and the minimal eigenvalue of the symmetric part of the unperturbed Schur complement matrix S. In Sect. 4, we show estimates of all these values for the finite element Oseen problem.

4 Properties of Matrices A and $\widetilde{S}$

The dependence of the critical constants c_A, C_A, ε_E and c_S from Theorem 1 on the problem and discretization parameters can be given explicitly. The analysis exploits the SUPG-FE origin of matrix A (matrix C is zero in the inf-sup FE method). Let

$\{\varphi_i\}_{1\le i\le n}$ and $\{\psi_j\}_{1\le j\le m}$ be bases of $\mathbb{V}_h$ and $\mathbb{Q}_h$, respectively. From the definition of matrix A and for arbitrary $v \in \mathbb{R}^n$ and corresponding $\boldsymbol{v}_h = \sum_{i=1}^n v_i\varphi_i$, one gets the following identity:

$$\langle Av, v\rangle = \alpha\|\boldsymbol{v}_h\|^2 + \nu\|\nabla\boldsymbol{v}_h\|^2 + \sum_{\tau\in T_h}\sigma_\tau\|\boldsymbol{w}\cdot\nabla\boldsymbol{v}_h\|_\tau^2 + \frac{1}{2}\int_{\Gamma_{\mathrm{N}}}(\boldsymbol{w}\cdot\boldsymbol{n})|\boldsymbol{v}_h|^2\,ds - \frac{1}{2}\sum_{\tau\in T_h}((\operatorname{div}\boldsymbol{w})\boldsymbol{v}_h, \boldsymbol{v}_h)_\tau + \sum_{\tau\in T_h}\sigma_\tau(\alpha\boldsymbol{v}_h - \nu\Delta\boldsymbol{v}_h, \boldsymbol{w}\cdot\nabla\boldsymbol{v}_h)_\tau, \tag{12}$$

where $\boldsymbol{n}$ is the outward normal on Γ_{N}. For a detailed discussion of the role each term from (12) plays in determining properties of matrix A, we refer to [16, 17]. Here we dwell on the last term in (12) due to the SUPG stabilization. The ν-dependent part of it vanishes for P1 finite element velocities, but not for most of inf-sup stable pressure–velocity pairs. Both analysis and numerical experiments below show that this term may significantly affect the properties of the matrix A, leading to unstable behavior of incomplete LU factorization unless the stabilization parameters are chosen sufficiently small.

The estimates for ellipticity and stability constants for A and $\widetilde{S}$ are summarized in Theorem 2. In order to formulate the theorem, we recall several well-known estimates. First, recall the Sobolev trace inequality

$$\int_{\Gamma_{\mathrm{N}}}|v|^2\,ds \le C_0\|\nabla v\|^2 \quad \forall\, v\in H^1(\Omega),\ v = 0 \text{ on } \partial\Omega\setminus\Gamma_{\mathrm{N}}. \tag{13}$$

For any tetrahedron $\tau \in T_h$ and arbitrary $\boldsymbol{v}_h \in \mathbb{V}_h$, the following FE trace and inverse inequalities hold

$$\int_{\partial\tau}\boldsymbol{v}_h^2\,ds \le C_{\mathrm{tr}}h_\tau^{-1}\|\boldsymbol{v}_h\|_\tau^2,\ \|\nabla\boldsymbol{v}_h\|_\tau \le C_{\mathrm{in}}h_\tau^{-1}\|\boldsymbol{v}_h\|_\tau,\ \|\Delta\boldsymbol{v}_h\|_\tau \le \bar{C}_{\mathrm{in}}h_\tau^{-1}\|\nabla\boldsymbol{v}_h\|_\tau, \tag{14}$$

where the constants C_{tr}, C_{in}, $\bar{C}_{\mathrm{in}}$ depend only on the polynomial degree k and the shape regularity constant C_T from (4). In addition, denote by C_{f} the constant from the Friedrichs inequality:

$$\|\boldsymbol{v}_h\| \le C_{\mathrm{f}}\|\nabla\boldsymbol{v}_h\| \quad \forall\boldsymbol{v}_h\in\mathbb{V}_h, \tag{15}$$

and let $C_{\boldsymbol{w}} := \|(\boldsymbol{w}\cdot\boldsymbol{n})_-\|_{L^\infty(\Gamma_{\mathrm{N}})}$. We introduce the velocity mass and stiffness matrices M and K: $M_{ij} = (\varphi_i, \varphi_j)$, $K_{ij} = (\nabla\varphi_i, \nabla\varphi_j)$ and the pressure mass matrix M_p: $(M_p)_{ij} = (\psi_i, \psi_j)$.

Theorem 2 *Assume that $\boldsymbol{w} \in L^\infty(\Omega)$, problem and discretization parameters satisfy*

$$\begin{cases} C_{\boldsymbol{w}} C_{\mathrm{tr}} h_{\min}^{-1} \le \dfrac{\alpha}{4} \quad or \quad C_{\boldsymbol{w}} C_0 \le \dfrac{\nu}{4}, \\ \|\mathrm{div}\, \boldsymbol{w}\|_{L^\infty(\Omega)} \le \dfrac{1}{4} \max\{\alpha, \nu C_f^{-1}\}, \\ \sigma_\tau \le \dfrac{h_\tau^2}{2\nu \bar{C}_{\mathrm{in}}^2} \left(1 + \dfrac{\alpha h_\tau^2}{\nu C_{\mathrm{in}}^2}\right) \quad and \quad \sigma_\tau \le \dfrac{h_\tau}{4\|\boldsymbol{w}\|_{L^\infty(\tau)} C_{\mathrm{in}}} \quad \forall \tau \in T_h, \end{cases} \tag{16}$$

with constants defined in (13)–(15)*. Then the matrix A is positive definite and the constants* c_A*,* C_A*,* c_S *and* ε_E *can be estimated as follows:*

$$\begin{aligned} c_A &\ge \frac{1}{4} \lambda_{\min}(\alpha M + \nu K), \\ C_A &\le c \left(1 + \frac{\|\boldsymbol{w}\|_{L^\infty(\Omega)}}{\sqrt{\nu\alpha} + \nu + h_{\min}\alpha}\right), \\ c_S &\ge \frac{c\, \lambda_{\min}(M_p)}{(\nu + \alpha + \|\boldsymbol{w}\|_{L^\infty(\Omega)} + \|\mathrm{div}\boldsymbol{w}\|_{L^\infty(\Omega)})(1 + C_A^2)}, \\ \varepsilon_E &\le \left(\frac{\bar{\sigma}}{2\nu} \lambda_{\max}(M_p)\right)^{\frac{1}{2}}, \end{aligned} \tag{17}$$

where c is a generic constant independent of problem and discretization parameters.

Theorem 2 shows that matrices A and $\widetilde{S}$ are positive definite if conditions (16) on the parameters of the finite element method are satisfied. In this case, the matrix in (3) admits LU factorization without pivoting. The *first condition* in (16) is trivially satisfied with $C_{\boldsymbol{w}} = 0$ if $\Gamma_{\mathrm{N}} = \varnothing$ or the entire Γ_{N} is outflow boundary. However, we know that this is often not the case for the hemodynamics problems (see item (ii) in the introduction). On the other hand, small time step results in a large value of α which eases the first condition. The *second condition* is specific for finite element approximations. The given $\boldsymbol{w}$ approximates velocity field of an incompressible fluid and hence one intuitively expects $\|\mathrm{div}\boldsymbol{w}\|_{L^\infty(\Omega)}$ decreases for a refined grid (a rigorous proof may not be straightforward for lower order finite elements). However, the $\boldsymbol{w}$-divergence norm depends on fluid velocity field and may be large for ν small enough. Fortunately, for small Δt the second condition holds due to $\alpha \sim (\Delta t)^{-1}$. The *third condition* in (16) appears due to the stabilization included in the finite element formulation (6). The same or a similar condition on stabilization parameters appears in the literature on the analysis of SUPG stabilized methods for the linearized Navier–Stokes equations, see, e.g., [21]. The reason is that the positive definiteness of A is equivalent to the coercivity of the velocity part of the bilinear form from (6), which is crucial for deriving finite element method error estimates. Therefore, stabilization parameter design suggested in the literature typically satisfies $\sigma_\tau \lesssim h_\tau^2/\nu$ and $\sigma_\tau \lesssim h_\tau/\|\boldsymbol{w}\|_{L^\infty(\tau)}$ *asymptotically*, i.e. up to a scaling factor independent of discretization parameters. As follows from (8), the conditions (16) on the SUPG stabilization parameters (7) are valid if $\bar{\sigma} \le \min\{\bar{C}_{\mathrm{in}}^{-2}, \frac{1}{2} C_{\mathrm{in}}^{-1}\}$. Moreover, the value of the $\bar{\sigma}$ parameter from the SUPG term is crucial for the bound on ε_E which measures

the discrepancy between B and $\widetilde{B}$. Thanks to (11) and Theorem 1 we see that ε_E has to be small enough to guarantee the stability of the factorization. Numerical results will support this observation. This puts additional implicit restrictions on $\bar{\sigma}$.

The domain anisotropy, see item (i) in the introduction, affects the lower bound for c_S in Theorem 2. The generic constant c in this bound depends on the inf-sup constant for $\mathbb{V}_h - \mathbb{Q}_h$ pair. Nevertheless, we shall see from experiments that the incomplete LU preconditioning in practice remains stable and efficient for stretched domains. Numerical experiments also show that the preconditioner has remarkable adaptivity properties with respect to different flow regimes, see item (iii) in the introduction. The bounds in Theorem 2 depend on $\boldsymbol{w}$ and ν, and hence on the Reynolds number. We observed in practice that the preconditioning remains stable over the range of Reynolds number and the fill-in adaptively increases or decreases in such a way that the number of iterations remains nearly the same.

5 Two-Parameter Threshold ILU Factorization

Incomplete LU factorizations of (3) can be written in the form $A = LU - E$ with an error matrix E. How small is the matrix E can be ruled by the choice of a threshold parameter $\tau > 0$. The error matrix E is responsible for the quality of preconditioning, see, for example, [15] for estimates on GMRES method convergence written in terms of $\|E\|$ and subject to a proper pre-scaling of A and the diagonalizability assumption. In general, the analysis of ILU factorization is based on the following arguments. For positive definite matrices A one can choose such a small τ that the product LU of its incomplete triangular factors L and U is also positive definite and so estimates from [11] can be applied to assess the numerical stability of the incomplete factorization: for $c_A = \lambda_{\min}(A_S)$, the sufficient condition is $\tau < c_A n^{-1}$. In practice, however, larger τ are used.

Theorem 2 shows that for certain flow regimes and for the choice of stabilization parameters the ellipticity constants c_A and c_S for A and S, respectively, approach zero. This may imply that the ILU factorization of (3) becomes unstable if possible at all. To ameliorate the performance of the preconditioning, we consider the two-parameter Tismenetsky–Kaporin variant of the threshold ILU factorization. The factorization was introduced and first studied in [14, 23, 24] for symmetric positive definite matrices and recently for non-symmetric matrices in [16, 17].

Given a matrix $A \in \mathbb{R}^{n\times n}$, the two-parameter factorization can be written as

$$A = LU + LR_u + R_\ell U - E, \tag{18}$$

where R_u and R_ℓ are strictly upper and lower triangular matrices, while U and L are upper and lower triangular matrices, respectively. Given two small parameters $0 < \tau_2 \le \tau_1$ the off-diagonal elements of U and L are either zero or have absolute values greater than τ_1, the absolute values of R_ℓ and R_u entries are either zero or belong to $(\tau_2, \tau_1]$; entries of the error matrix are of order $O(\tau_2)$. We refer to (18)

as the ILU(τ_1, τ_2) factorization of A. In the particular case of $\tau_1 = \tau_2$, factorization ILU(τ_1,τ_2) is equivalent to the well-known ILUT(p, τ) dual parameter incomplete factorization [22] with $p = n$ (all elements passing the threshold criterion are kept in the factors). If no small pivots modification is done, the only differences between the algorithms (for $\tau_1 = \tau_2$ and $p = n$) are different scaling of pivots and row dependent scaling of threshold values. The two-parameter ILU factorization goes over a ILUT(n, τ) factorization: the fill-in of L and U is ruled by the first threshold parameter τ_1, while the quality of the resulting preconditioner is mainly defined by τ_2, once $\tau_1^2 \lesssim \tau_2$ holds. In other words, the choice $\tau_2 = \tau_1^2 := \tau^2$ may provide the fill-in of ILU(τ_1, τ_2) to be similar to that of ILUT(n, τ), while the convergence of preconditioned Krylov subspace method is better and asymptotically (for $\tau \to 0$) can be comparable to the one with ILUT(n, τ^2) preconditioner. For symmetric positive definite matrices this empirical advantages of ILU(τ_1, τ_2) are rigorously explained in [14], where estimates on the eigenvalues and K-condition number of $L^{-1}AU^{-1}$ were derived with $L^T = U$ and $R_\ell^T = R_u$. The price one pays is that computing L, U factors for ILU(τ_1, τ_2) is computationally more costly than for ILUT(n, τ_1), since intermediate calculations involve the entries of R_u. However, this factorization phase of ILU(τ_1, τ_2) is still less expensive than that of ILUT(n, τ_2). A pseudo-code of the row-wise ILU(τ_1, τ_2) factorization can be found in [16].

Analysis of the decomposition (18) of a general non-symmetric matrix is limited to simple estimate (2.5) from [10] applied to the matrix $(L + R_\ell)(U + R_u) = A + R_\ell R_u + E$. The lower bound for the pivots of the (18) factorization is the following:

$$|L_{ii}U_{ii}| \geq \min_{v\in\mathbb{R}^n} \frac{\langle (A + R_\ell R_u + E)v, v\rangle}{\|v\|^2} \geq c_A - \|R_\ell R_u\| - \|E\|, \qquad (19)$$

with the ellipticity constant c_A and the norms $\|R_\ell R_u\|$ and $\|E\|$ proportional to τ_1^2 and τ_2, respectively. Hence, we may conclude that the numerical stability of computing for $L^{-1}x$ and $U^{-1}x$ is ruled by the second parameter and the *square* of the first parameter, while the fill-in in both factors is defined by τ_1 rather than τ_1^2. The Oseen problem setup may be such that the estimates from Theorem 2 predict that the coercivity constant c_A and the ellipticity constant c_S are small. This increases the probability of the breakdown of ILUT(n, τ) factorization of the saddle-point matrix $\mathscr{A}$, and demonstrates the benefits of ILU(τ_1, τ_2) factorization.

The final important remark in this section is that in all computations we use the simple preprocessing of matrix $\mathscr{A}$ by the two-side scaling as described in [16].

6 Numerical Results

The model hemodynamic problem of interest is a blood flow in a right coronary artery. To set up the problem, we use the geometry recovered from a real patient coronary CT angiography. The 3D vessel is branching and is cut to embed in the box 6.5 cm × 6.8 cm × 5 cm, see Fig. 1. The diameter of the inlet cross-section is about

Fig. 1 The coarse (63k, left) and fine (120k, right) grids in the right coronary artery. The bottom figures zoom a part of the domain

0.27 cm. We generate two tetrahedral meshes using ANI3D package [2]. The meshes shown in Fig. 1 consist of 63k and 120k tetrahedra. The Navier–Stokes system (1) is integrated in time using a semi-implicit second order method with $\Delta t = 0.005$. This and the discretization with Taylor–Hood (P2-P1) finite elements result in a sequence of discrete Oseen problems (3). The algebraic systems have nearly 300k and 600k unknowns for the coarse and the fine meshes, respectively. Other model parameters are $\nu = 0.04\,\mathrm{cm}^2/\mathrm{s}$, $\rho = 1\,\mathrm{g/cm}$. We integrate the system over one cardiac cycle, which is 0.735 s. The inlet velocity waveform [13] shown in Fig. 2 defines the Poiseuille flow rate through the inflow cross-section. The figure shows the integral average of the normal velocity component over the inflow boundary. The vessel walls were treated as rigid and homogeneous Dirichlet boundary conditions for the velocity are imposed on the vessel walls. On all outflow boundaries we set the normal component of the stress tensor equal to zero. For the suitable choice of stabilization parameters, cf. below, the computed FE solutions are physically meaningful, see Fig. 3.

We study the performance of the ILU(τ) factorization for different values of discretization, stabilization, and threshold parameters. For numerical test we use the implementation of ILU(τ_1, τ_2) available in the open source software [1, 2]. The values

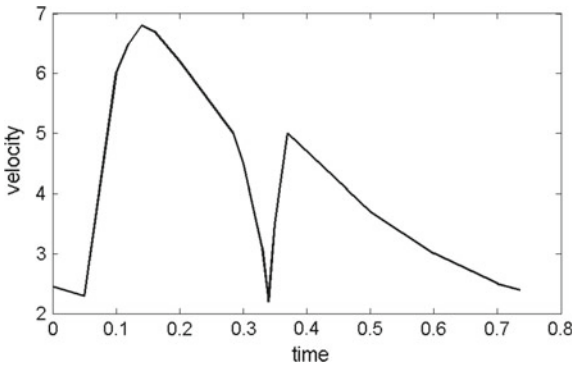

Fig. 2 The averaged velocity waveform on the inflow as a function of time in the right coronary artery

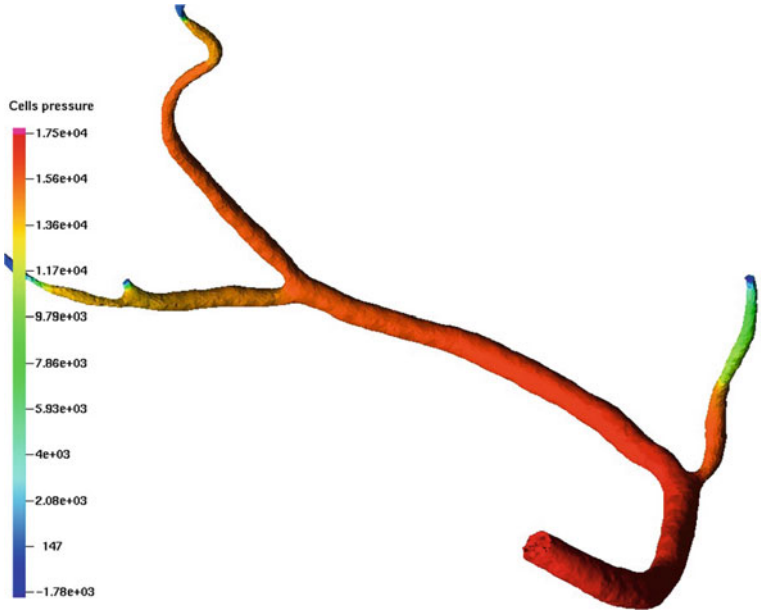

Fig. 3 The pressure distribution in the right coronary artery at time 0.15 s

of ILU thresholds $\tau_1 = 0.03$, $\tau_2 = 7\tau_1^2$ are taken from [16]. In that paper this design of threshold parameters was found to be close to optimal for a range of problems and fluid parameters. In all experiments we use BiCGstab method with the right preconditioner defined by the ILU(τ_1,τ_2) factorization.

Table 1 shows the total number of the preconditioned BiCGstab iterations #it, the total number of modifications of nearly zero pivots #pmod, the fill-in ratio and the CPU times (factorization time T_{build}, iteration time T_{it}, total solution CPU time

Table 1 The performance of ILU ($\tau_1 = 0.03$, $\tau_2 = 7\tau_1^2$) for right coronary artery. The number of iterations and pivot modifications and the solution stages times accumulated for 147 time steps

Mesh	$\bar{\sigma}$		fill_{LU}	pmod	#it	T_{build}	T_{it}	T_{CPU}
63k	0	Min	0.711	0	131	2.64	13.59	16.55
		Average	0.854	0	142.2	3.82	15.42	19.24
		Max	1.009	0	164	5.16	17.47	22.11
		Total	–	0	20908	562	2267	2829
63k	1/12	Min	0.711	0	125	2.63	13.03	16.10
		Average	0.838	0	138.0	3.65	14.84	18.49
		Max	0.980	0	156	4.85	22.62	26.42
		Total	–	0	20292	537	2182	2719
120k	0	Min	0.738	0	163	6.32	36.96	43.93
		Average	0.846	0	178.2	8.46	42.09	50.56
		Max	0.985	0	220	11.17	61.61	71.34
		Total	–	0	26209	1244	6188	7432
120k	1/12	Min	0.738	0	158	6.27	35.88	42.35
		Average	0.832	1	179.9	8.11	41.71	49.83
		Max	0.959	18	357	10.51	87.58	97.94
		Total	–	21	26446	1192	6132	7325

$T_{\text{CPU}} = T_{\text{build}} + T_{\text{it}}$) needed to perform 147 time steps. The fill-in ratio is defined by $\text{fill}_{LU} = (\text{nz}(L) + \text{nz}(U))/\text{nz}(A)$, where $\text{nz}(A) = \sum_{ij} \text{sign}|A_{ij}|$. On every time step, the Krylov subspace iterations are done until the initial residual is reduced by 10 orders of magnitude. The initial guess in the solver is the extrapolated solution from the previous time step. We generate sequences of the discrete Oseen problems (2) with ($\bar{\sigma} = 1/12$) and without ($\bar{\sigma} = 0$) SUPG-stabilization. In both cases, the 'quasi-optimal' choice of parameters τ_1, τ_2 leads to stable computations over the whole cardiac cycle. The total number of iterations depends on the mesh and appears to be very similar for both examples with and without stabilization. The total number of iterations is 20% larger for the fine grid, which should be expected for the preconditioner based on an incomplete factorization.

The time history of the statistics from Table 1 is shown in Figs. 4 and 5. It is interesting to note that the graph of the fill-in ratio for the LU-factors and the graph of the ILU factorization time repeat surprisingly well the waveform of the inflow velocity, see the two top plots in Figs. 4 and 5. This explains the rather modest variation of the iteration counts and CPU times per linear solve over the cardiac cycle, see the two bottom plots in Figs. 4 and 5. Note that the fill-in ratio $\text{fill}_{LU} < 1$ means that the number of non-zero elements in factors is less then in ILU(0), the commonly used ILU factorization by position. The fact that fill-in of the L and U blocks decreases or increases depending on the Reynolds number is the remarkable adaptive property of the two-parameter ILU preconditioner which makes it very competitive to other state-of-the-art preconditioners. The difference in otherwise similar performance of

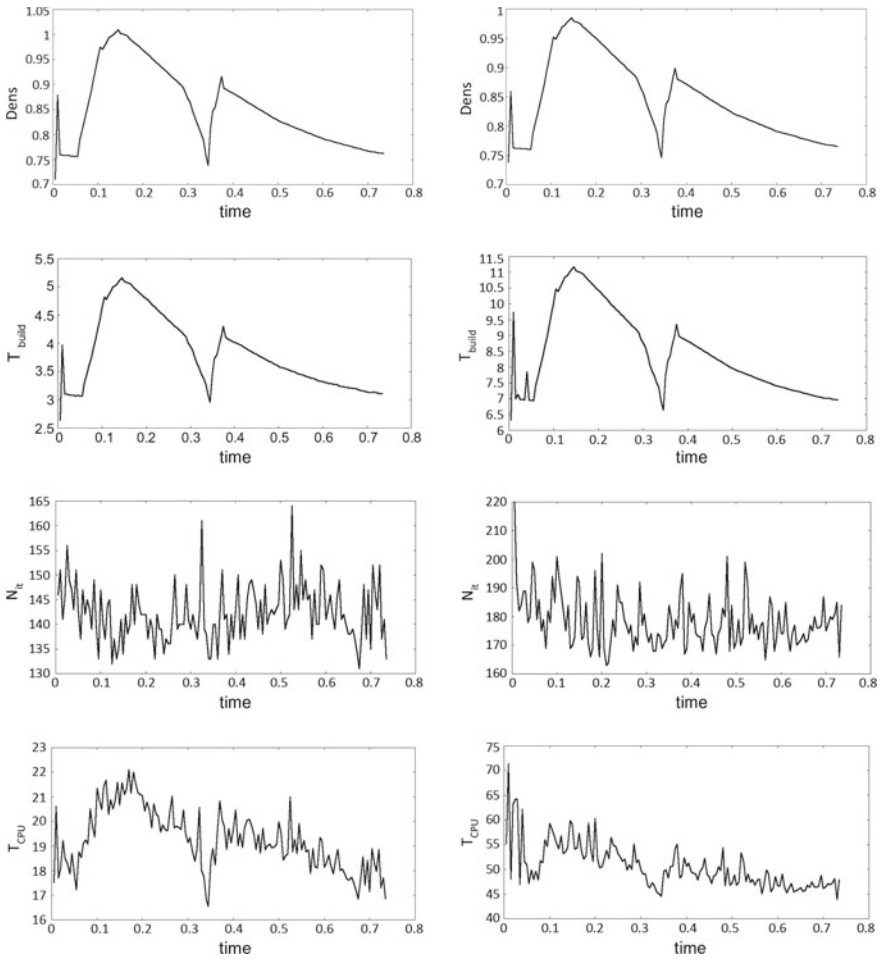

Fig. 4 Right coronary artery, computations on grid 63k (left) and grid 120k (right) without SUPG-stabilization and $\tau_1 = 0.03$: The plots (from top to bottom) show the density of the preconditioner (fill-in ratio), the time of ILU factorization, the number of BiCGStab iterations, the total CPU time of the linear system solution at each time step

linear solvers for the cases $\bar{\sigma} = 1/12$ and $\bar{\sigma} = 0$ is the following: For $\bar{\sigma} = 1/12$, when the maximum flow rate on the inlet is achieved, the number of iterations and times needed to build preconditioner increase essentially (approximately twice as much as average). This happens over a few time steps. In these cases when factorization is performed several small pivots occur and their modification is performed during the incomplete factorization.

In the second series of experiments, we demonstrate practical importance of restrictions (16) on σ_τ. The Theorems 1 and 2 state that the existence of exact stable LU factorization of $\mathscr{A}$ (almost) without pivoting is guaranteed for σ_τ small

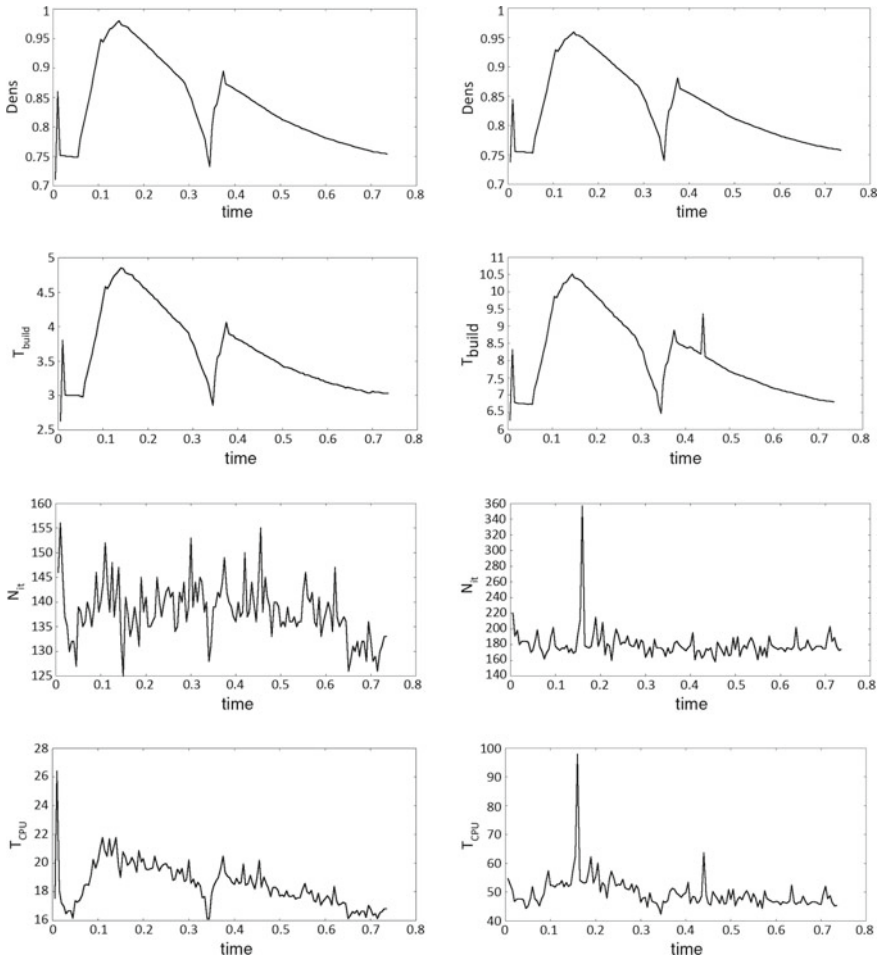

Fig. 5 Right coronary artery, computations on grid 63k (left) and grid 120k (right), SUPG-stabilization with $\bar{\sigma} = 1/12$ and $\tau_1 = 0.03$: The plots (from top to bottom) show the density of the preconditioner (fill-in ratio), the time of ILU factorization, the number of BiCGStab iterations, the total CPU time of the linear system solution at each time step

enough. The estimate (8) explains why σ_τ from (7) with $\bar{\sigma} \le \min\{\bar{C}_{\text{in}}^{-2},\ \frac{1}{2}C_{\text{in}}^{-1}\}$ satisfies (16). The previous series of experiments show that for the stabilization parameter $\bar{\sigma} = 1/12$ the factorization is done on both meshes without pivot modifications even for the relatively large value of the threshold, $\tau_1 = 0.03$. Now we increase the value of the stabilization parameter and take $\bar{\sigma} = 1/6$. Table 2 reports on the performance of ILU($\tau_1, \tau_2 = 7\tau_1^2$) preconditioner for the sequence of the SUPG-stabilized Oseen systems generated on the coarse grid with $\bar{\sigma} = 1/6$. The choice of the threshold as small as $\tau_1 = 10^{-4}$ produces the factorization close to the exact one. Hence, the average number of BiCGstab iterations is only 8. Although no pivot modifications

Table 2 The performance of ILU (τ_1, $\tau_2 = 7\tau_1^2$) for right coronary artery, $\bar{\sigma} = 1/6$, coarse mesh 63 k

τ_1		fill_{LU}	pmod	#it
0.0003	Min	5.978	0	7
	Average	8.466	1	12.2
	Max	11.206	12	135
	Total	–	16	1806
0.0001	Min	8.716	0	5
	Average	12.557	0	8.1
	Max	16.742	0	100
	Total	–	0	1198

Table 3 The performance of ILU (τ_1, $\tau_2 = 7\tau_1^2$) for right coronary artery with different viscosities ν. The table shows values of τ_1 which allow to run the simulation for the complete cardiac cycle for different parameters $\bar{\sigma}$. '$\star$' means finite element solution blow-up, '–' means intractable systems for any possible τ_1

ν, $\backslash\bar{\sigma}$ (cm^2/s)	0	1/96	1/48	1/24	1/12	1/6	1/3
0.040	0.03	0.03	0.03	0.03	0.03	0.03	0.003
0.025	$\star$	0.03	0.03	0.03	0.03	0.003	–

occurred, the fill-in ratio is unacceptably large and on some time steps the number of iterations may be large either. The observation that two-parameter ILU needs no pivoting with $\tau_1 = 10^{-4}$ suggests that the exact factorization is stable. For larger values of the threshold parameter, $\tau_1 = 3 \times 10^{-4}$, the fill-in ratio naturally decreases and the average number of BiCGstab iterations increases. Now, on two time steps the algorithm has to make 12 and 4 modifications of nearly zero pivots in order to avoid the breakdown. The pivot modifications causes the convergence slowdown, the maximum number of iterations in the Krylov subspace solver grows up to 135 iterations. Furthermore, on the *finer* grid certain Oseen systems with $\bar{\sigma} = 1/6$ can not be solved by the ILU-preconditioned BiCGstab iterations with any values of the threshold parameter which we tried.

We repeat the same simulations on the coarse grid, but for a smaller value of the viscosity coefficient, $\nu = 0.025\,\text{cm}^2/\text{s}$. For this viscosity, the simulation without SUPG stabilization fails (solution blows up at $t = 0.23$ s). Stabilization is necessary and adding it allows to obtain physiologically meaningful solution. At the same time, for larger parameter $\bar{\sigma}$ the linear systems are harder to solve. Indeed, $\bar{\sigma} = 1/6$ requires smaller threshold parameter τ_1, whereas $\bar{\sigma} = 1/3$ generates unsolvable systems, see Table 3. This experiment confirms that restrictions on $\bar{\sigma}$ come both from stability of the FE method and algebraic stability of the LU factorization. Both restrictions have to be taken into account when one decides about the choice of stabilization parameters.

Table 4 The performance of plain ILU (τ_1, τ_2) preconditioning versus reusing the same preconditioner over two time steps

	#it	T_{build}	T_{it}	T_{CPU}
Building preconditioner each time step	138	4.2	14.8	18.9
Building preconditioner every second time step	139	2.1	15.1	17.2

We also experiment with reusing ILU preconditioner over several time steps. This looks like a reasonable thing to try, since the time step is small and the system may not change too much from one time step to another one. Numerical results, however, show that the time cost of the setup phase of the preconditioner is small compared to the time needed by the Krylov subspace method to converge. Hence this strategy gives some time saving, but a moderate one. To illustrate this, we show in Table 4 the averaged data for the number of iterations per time step, the setup time needed to compute L and U factors, the time required by the Krylov subspace solver, and the total time, which is the sum of those two. The data is shown for the flow in the artery with the 63 K grid, $\nu = 0.04, \bar{\sigma} = 1/12, \tau_1 = 0.03, \tau_2 = 7\tau_1^2$. We see that reusing the same preconditioner over two time steps saves about 10% of the total computational time.

7 Conclusions

In this paper we studied the preconditioner based on elementwise incomplete two-parameter threshold ILU factorization of non-symmetric saddle-point matrices. The Krylov subspace solver with the preconditioner was used to simulate a blood flow in a right coronary artery reconstructed from a real patient coronary CT angiography. We tested the method for a range of physiological and discretization parameters. Several conclusions can be made: The solver efficiently handles typical features of hemodynamic applications such as geometrically stretched domains, variable flow regimes, and open boundary conditions with possible reversed flows. The preconditioner benefits from smaller time increments. One can reuse the preconditioner over several time steps, although for this particular application the benefit of doing this is modest, since the setup phase of the preconditioning is cheap compared to the time cost of iterations. A sequential version of the preconditioner is straightforward to implement for any type of finite elements and other discretizations once the matrix entries are available. For parallel computations it is natural to combine the ILU preconditioner with the additive Schwarz method. This is a subject of our further research.

Acknowledgements The experimental part of this work has been supported by the Russian Science Foundation through the grant 14-31-00024. The theoretical part (the contribution of the second author) was partially supported by NSF grant DMS1522252.

References

1. Advanced Numerical Instruments 2D. http://sourceforge.net/projects/ani2d
2. Advanced Numerical Instruments 3D. http://sourceforge.net/projects/ani3d
3. Benzi M, Deparis S, Grandperrin G, Quarteroni A (2016) Parameter estimates for the relaxed dimensional factorization preconditioner and application to hemodynamics. Comput Methods Appl Mech Engrg 300:129–145
4. Benzi M, Golub GH, Liesen J (2005) Numerical solution of saddle point problems. Acta Numer 14:1–137
5. Bodnár T, Galdi GP, Nečasová Š (eds) (2014) Fluid-structure interaction and biomedical applications. Birkhäuser, Basel
6. Chizhonkov EV, Olshanskii MA (2000) On the domain geometry dependence of the LBB condition. M2AN Math Model Numer Anal 34(5):935–951
7. Deparis S, Grandperrin G, Quarteroni A (2014) Parallel preconditioners for the unsteady Navier-Stokes equations and applications to hemodynamics simulations. Comput Fluids 92:253–273
8. Elman HC, Silvester DJ, Wathen AJ (2014) Finite elements and fast iterative solvers: with applications in incompressible fluid dynamics, 2nd edn. Oxford University Press, Oxford
9. Girault V, Raviart P-A (1979) Finite element approximation of the Navier-Stokes equations, vol 749. Lecture Notes in Mathematics. Springer, Berlin
10. Golub GH, Van Loan C (1979) Unsymmetric positive definite linear systems. Linear Algebra Appl 28:85–97
11. Golub GH, Van Loan CF (1996) Matrix computations, 3rd edn. Johns Hopkins University Press, Baltimore
12. Hou G, Wang J, Layton A (2012) Numerical methods for fluid-structure interaction—a review. Commun Comput Phys 12(2):337–377
13. Jung J, Hassanein A, Lyczkowski RW (2006) Hemodynamic computation using multiphase flow dynamics in a right coronary artery. Ann Biomed Engrg 34(3):393–407
14. Kaporin IE (1998) High quality preconditioning of a general symmetric positive definite matrix based on its $U^TU + U^TR + R^TU$-decomposition. Numer Linear Algebra Appl 5(6):483–509
15. Kaporin IE (2007) Scaling, reordering, and diagonal pivoting in ILU preconditionings. Russ J Numer Anal Math Model 22(4):341–376
16. Konshin IN, Olshanskii MA, Vassilevski YV (2015) ILU preconditioners for nonsymmetric saddle-point matrices with application to the incompressible Navier-Stokes equations. SIAM J Sci Comput 37(5):A2171–A2197
17. Konshin IN, Olshanskii MA, Vassilevski YV (2016) LU factorizations and ILU preconditioning for stabilized discretizations of incompressible Navier-Stokes equations. Numerical Analysis and Scientific Computing Preprint Seria 49, University of Houston
18. Nordsletten D, Smith N, Kay D (2010) A preconditioner for the finite element approximation to the arbitrary Lagrangian-Eulerian Navier-Stokes equations. SIAM J Sci Comput 32(2):521–543
19. Olshanskii MA, Tyrtyshnikov EE (2014) Iterative methods for linear systems: theory and applications. SIAM, Philadelphia
20. Passerini T, Quaini A, Villa U, Veneziani A, Canic S (2013) Validation of an open source framework for the simulation of blood flow in rigid and deformable vessels. Int J Numer Methods Biomed Engrg 29(11):1192–1213
21. Roos H-G, Stynes M, Tobiska L (1996) Numerical methods for singularly perturbed differential equations: convection-diffusion and flow problems. Springer, Berlin
22. Saad Y (2003) Iterative methods for sparse linear systems, 2nd edn. SIAM, Philadelphia
23. Suarjana M, Law KH (1995) A robust incomplete factorization based on value and space constraints. Int J Numer Methods Engrg 38(10):1703–1719
24. Tismenetsky M (1991) A new preconditioning technique for solving large sparse linear systems. Linear Algebra Appl 154(156):331–353